

A mesoscopic approach for multi-phase flows in nano-corrugated channels

R. Benzi,¹ L. Biferale,¹ M. Sbraglia,² S. Succi,³ and F. Toschi^{3,4}

¹*Dipartimento di Fisica and INFN, Università di Roma “Tor Vergata”,
Via della Ricerca Scientifica 1, 00133 Roma, Italy.*

²*Department of Applied Physics, University of Twente,
P.O. Box 217, 7500 AE Enschede, The Netherlands*

³*Istituto per le Applicazioni del Calcolo CNR, Viale del Policlinico 137, 00161 Roma, Italy.*

⁴*INFN, Sezione di Ferrara, via G. Saragat 1, I-44100, Ferrara, Italy.*

(Dated: September 26, 2018)

An approach based on a lattice version of the Boltzmann kinetic equation for describing multi-phase flows in nano- and micro-corrugated devices is proposed. We specialize it to describe the wetting/dewetting transition of fluids in presence of nanoscopic grooves etched on the boundaries. This approach permits to retain the essential *supra-molecular* details of fluid-solid interactions without surrendering -actually boosting- the computational efficiency of continuum methods. The mesoscopic method is first validated quantitatively against Molecular Dynamics (MD) results of *Cottin-Bizonne et al.* [Nature Mater. **2** 237 (2003)] and then applied to more complex situations which are hardly accessible to MD simulations. The resulting analysis confirms that surface roughness and capillary effects may conspire to promote a counter-intuitive but significant reduction of the flow drag with substantial enhancement in the mass flow rates and slip-lengths in the micrometric range for highly hydrophobic surfaces.

PACS numbers: 83.50.Rp,68.03.Cd,05.20.Dd,02.70.Ns

The motion of fluids at the micro and nanoscale is controlled by the competition of dissipative effects and pressure drive. The weakness of inertia in the microworld implies that it is increasingly difficult to push fluids across micro/nanoconfined geometries, as their surface/volume ratio is made larger and larger. An obvious consequence is that the dynamics of microflows is crucially affected by the interaction of the fluid with the confining solid boundaries. Information on these interactions is usually conveyed into the formulation of proper boundary conditions for the fluid flow. In particular, slippage properties (see [2] for a recent review) have been reported in experiments and in molecular dynamics simulations, depending on the thermodynamical and wetting properties of the boundary (contact angle) and on the surface geometry [1, 3, 4, 5, 6, 7, 8, 9]. A fundamental question arises as to whether the fluid really slips over the surface, or rather the indirect measurements based on pressure/mass flow rate relations or surface force apparatus reflect an apparent slip arising from surface inhomogeneities or complex interface with additional physics. Indeed, it has been argued that a gas layer at the interface would alter the fluid dynamics in the bulk, leading to a mass flow rate increase even in the presence of pure no-slip [10, 11, 12, 22, 23]. This hypothesis is supported by the observation of nanobubbles trapped on the surface [13] and by a decreasing apparent slip length as the fluid is degassed [14].

The aim of this article is to discuss the complex effects, at the hydrodynamical scales, induced by the surface wetting properties in presence of complex geometries in micro- and nano-devices. The results can be summarized in two main points. First, we provide neat evidence that

the physics of the boundary conditions is quantitatively reproduced by modeling the fluid at mesoscopic level, by means of a minimal version of the Boltzmann equation, i.e. the Lattice Boltzmann Equation (LBE) [15, 16]. This result is obtained by performing a quantitative comparison of a “finite-volume” dewetting transition against recent Molecular Dynamics simulations (MD) [1, 17]. Far from being a mere technicality, this result opens the way to numerical investigations at spatial and time scales much larger than those currently available in most MD simulations. Second, we extend the MD results by investigating the critical dependency of the mass flow rate on the degree of roughness at constant bulk pressure. The simplest LBE reads as follows [19]:

$$f_i(\mathbf{x} + \mathbf{c}_i \Delta t, t + \Delta t) - f_i(\mathbf{x}, t) = -\omega \Delta t [f_i(\mathbf{x}, t) - f_i^{(eq)}(\mathbf{x}, t)] + F_i \Delta t, \quad (1)$$

where $f_i(\mathbf{x}, t)$ is the probability of finding a particle at site \mathbf{x} at time t , moving along one of the b -th lattice direction defined by the discrete speed \mathbf{c}_i with $i = 1, \dots, b$ and Δt is the time unit. The left-hand side of (1) stands for molecular free-streaming, whereas the right-hand side represents molecular collisions. These are expressed through a simple relaxation towards local Maxwellian equilibrium $f_i^{(eq)}$ in a time lapse of the order of $\tau \equiv \omega^{-1}$. Finally the term F_i represents a volumetric body-force, which can be tailored to produce highly non-trivial macroscopic effects, such as phase-transitions. Non-ideal effects, leading to two-phase flows, are modeled through a self-consistent force term:

$$\mathbf{F}(\mathbf{x}, t) = \mathcal{G}_b \sum_i w_i \psi(\mathbf{x}, t) \psi(\mathbf{x} + \mathbf{c}_i \Delta t, t) \mathbf{c}_i. \quad (2)$$

Here, $\psi(\mathbf{x})$ is a phenomenological pseudo-potential (generalized density), $\psi(\mathbf{x}, t) = \psi[\rho(\mathbf{x}, t)]$, first introduced by Shan and Chen [20], w_i are normalization weights and \mathcal{G}_b tunes the molecule-molecule interaction, i.e. it plays the role of the normalized *inverse temperature*, ϵ/KT , with ϵ the molecular interaction, K The Boltzmann constant and T the system temperature. Here we choose the standard form $\psi = \sqrt{\rho_0}\{1 - \exp(-\rho/\rho_0)\}$, with the reference density $\rho_0 = 1$, in lattice units.

In spite of its simplicity, the Shan-Chen approach provides two crucial ingredients of non-ideal fluid behavior: a non-ideal equation of state and a non-zero liquid-vapor surface tension, σ_{lv} . Both features are encoded in the expression of the non-ideal momentum flux tensor P_{kj} . In the hydrodynamic limit, the LBE equations (1)-(2) can be shown to evolve according to the Navier-Stokes equations [18] with a pressure tensor \overleftarrow{P} :

$$P_{kj} = \left[c_s^2 \rho + \frac{1}{2} c_s^2 \mathcal{G}_b \psi^2 + \frac{1}{2} c_s^4 \mathcal{G}_b \psi \Delta \psi + \frac{\mathcal{G}_b c_s^4}{4} |\nabla \psi|^2 \right] \delta_{kj} - \frac{1}{2} c_s^4 \mathcal{G}_b \partial_k \psi \partial_j \psi. \quad (3)$$

The equation of state in the bulk is $P = c_s^2 \rho + \frac{1}{2} c_s^2 \mathcal{G}_b \psi^2$ where we recognize a non-ideal contribution on top of the ideal equation of state $P = \rho c_s^2$ with c_s^2 the sound speed velocity. This equation of state supports a phase-transition at a critical density $\rho_c/\rho_0 = \ln(2)$, whenever the coupling strength exceeds (in magnitude) the critical value $\mathcal{G}_c = -4.0$. Concerning the velocity field, following [18], we set it to be zero at the boundary by using bounce-back boundary conditions while, for the case when slippage properties are a priori imposed, different boundary conditions should be used [25, 26]. Next, the

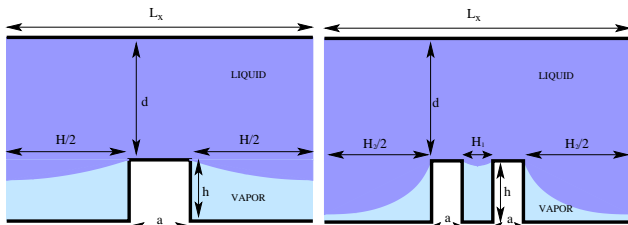


FIG. 1: Left: homogeneous roughness. A groove with depth $h = 33\Delta x$ and width $H = L_x - a$ (with $a = 10\Delta x$) is introduced on the bottom wall and periodic boundary conditions are assumed along x . In this configuration, the presence of vapor pockets inside the groove changes the “effective” boundary conditions felt by the bulk fluid, with a net decrease of drag when a pressure drop is applied. Right: channel with heterogeneous roughness. Two grooves of width $H_1 = 40\Delta x$ and $H_2 = 70\Delta x$ are present. The two grooves are filled separately at different values in the pressure/density diagram. The lattice spacing corresponds to $\Delta x \sim 0.3nm$.

density field $\rho(\mathbf{x})$ is assumed to match a given value $\psi_w = \psi(\rho_w)$, where ρ_w should be regarded as a free-parameter related to the strength of the fluid/solid in-

teractions. In [18] we have shown that by imposing the condition of mechanical equilibrium, $\partial_j P_{kj} = 0$, of the contact line separating the liquid, vapor and solid phases, one can compute analytically the *contact angle*, $\theta(\mathcal{G}_b, \rho_w)$. Notwithstanding their inherently mesoscopic character, the parameters \mathcal{G}_b and ρ_w carry no less physical content than their atomistic counterparts (relative strength of the attractive to repulsive interactions in MD simulations [9]). In order to study the wetting/dewetting transition on micro/nano-patterned surfaces (see Fig. 1) we have integrated the LBE equation (1) in a 2D Lattice using the nine-speed 2DQ9 model ($b = 9$), one of the most used 2D-LBE scheme, due to its superior stability [21, 24]. We have used the two geometries described in Fig. 1. All simulations have been performed at fixed “inverse temperature” $\mathcal{G}_b = -6.0$ i.e. beyond the critical value $\mathcal{G}_c = -4.0$. The relaxation parameter is taken as $\tau = 0.8$ in lattice units. The equation of state delivers the corresponding values of the liquid and gas density, $\rho_l = 2.65$ and $\rho_g = 0.07$ respectively, while the surface tension is $\sigma_{lv} = 0.105 \pm 0.002$ in lattice units. The value of the lattice spacing in physical units is obtained by matching the physical value of the liquid-vapor surface tension, with the one measured on the lattice, via the dimensional relation: $\sigma_{lv}^{phys} = KT/(\Delta x)^2 \sigma_{lv}$. For water/vapor at $T = 540^\circ$, where the density ratio is close to the values of our simulation, we have $\sigma_{lv}^{phys} = 0.022N/m$ which yields $\Delta x \sim 0.3nm$. This value is comparable with the atomic range of the Lennard-Jones potential used in MD. Molecular dynamics simulations have recently reported that the concerted effects of wetting phenomena and nano-corrugations can lead to a fairly substantial reduction of mechanical drag [1, 17]. Specifically, the authors in [1, 17] consider a nanometric channel flow with a regular sequence of longitudinal or transverse steps (with respect to the mean flow) along the solid wall of the channel, and show that, under suitable thermodynamic and geometric conditions, the presence of the steps triggers the formation of a gas film in the grooves within the obstacles. The liquid can then slide-away over the gas film, thereby experiencing a significantly reduced mechanical drag. Such phenomenon may occur only at a critical pressure drop between liquid and vapor phase, of the order of the capillary pressure, P_{cap} , given by the estimate: [17]:

$$P_{cap} = -\frac{2\sigma_{lv} \cos(\theta)}{L_x - a}. \quad (4)$$

In Fig. 2, we validate the LBE by a direct comparison with the MD results published in [1, 17] with the same geometry and with comparable contact angle. In particular, we show the Pressure drop between the bulk liquid and vapor phases $\Delta P_{lv} = P_l - P_v$, at changing the distance d (see Fig. 1) at fixed total mass, i.e. at changing the average density. As one can clearly see, the agreement between LBE and MD is quantitative. The plateaux ob-

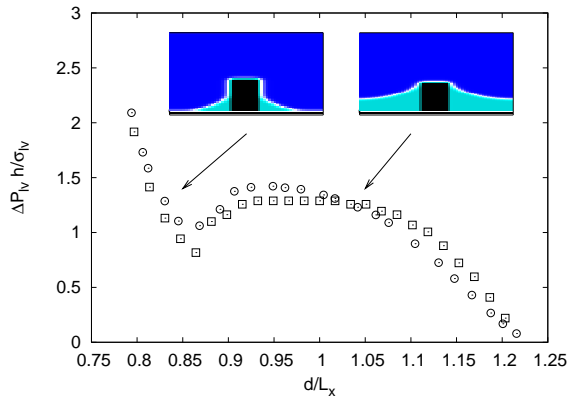


FIG. 2: Validation of our LBE simulation against MD results [17]. The LBE is done with the same aspect-ratios of MD. The dimensionless normalized pressure drop, $\Delta P_{lv} h / \sigma_{lv}$ between the two bulk phases, is shown as a function of the normalized distance d/L_x (see Fig. 1). LBE (\square) results have been obtained with a contact angle $\theta = 160^\circ$, which is consistent with the contact angle measured in MD (\circ) simulation (see Fig. 2 of [17]). The two insets represent the density configuration at the onset of the wetting/dewetting transition (right) and for a wetted configuration (left). The plateaux in the pressure curve defines the capillary pressure, P_{cap} .

served for ΔP_{lv} in the range $0.9 < d/L_x < 1.05$ corresponds to the pressure/density values at which the fluid is invading the corrugation, forming an interface which does not yet touch the bottom of the groove. This corresponds to the capillary pressure, P_{cap} . Reducing further d , i.e. increasing the average density, a change of concavity for $0.8 < d/L_x < 0.9$, is observed. This range corresponds to values such that the interface starts to touch the bottom of the groove, adjusting its pressure/density in such a way as to minimize the free energy in the presence of the new liquid-vapor-solid interface. The agreement of LBE with the capillary pressure (4) is checked in detail in Fig. 3, where we report the change of the pressure diagram with a changing distance d , for three different corrugation values, $L_x - a$. In the inset of Fig. 3, we extract the value of $\sigma_{lv} \cos(\theta)$ from the the slope of the observed plateaux *vs* $\Delta x / (L_x - a)$. The value of $\cos(\theta)$ is then obtained by estimating the surface tension, σ_{lv} , through Laplace’s law for a droplet in equilibrium with its saturated vapor. The agreement of the contact angle measured in this way, $\theta = 158^\circ \pm 6^\circ$, with the analytical estimate, $\theta = 160^\circ$, obtained in [18] by imposing the mechanical equilibrium condition of the contact line is very satisfactory.

The comparison shown in Fig. 2 and Fig. 3 demonstrates the first result discussed in this paper, namely that the model introduced in [18] captures the correct interplay between roughness and wetting effects.

Even more complex behavior is observed for heterogeneous nano-corrugations, with the simplest case shown

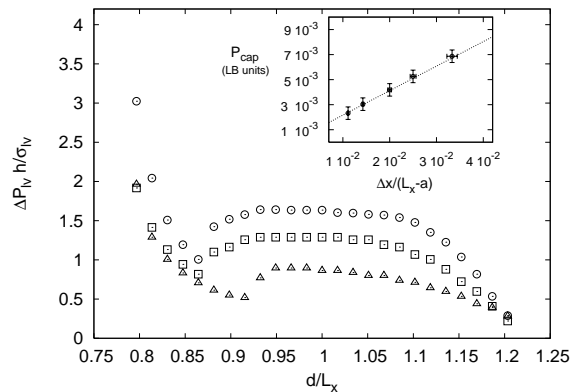


FIG. 3: Pressure variations at changing d for various roughnesses, $L_x = 50\Delta x$ (\triangle), $L_x = 60\Delta x$ (\square), $L_x = 80\Delta x$ (\circ) with $a = 10\Delta x$. In the inset, we show the relation (4). The slope is given by $2\sigma_{lv} \cos(\theta) = -0.196 \pm 0.006$ (LB units). With our surface tension $\sigma_{lv} = 0.105 \pm 0.002$ (LB units), this implies a best estimate of $\theta = 158^\circ \pm 6^\circ$.

in the right panel of Fig. 1. In this case, one has two characteristic groove sizes, H_1 and H_2 , and hence two corresponding critical capillary pressures. The pressure/density diagram for this heterogenous corrugation is shown in Fig. 4, where the two plateaux corresponding to the two capillary pressures coexist. This device may be considered a “smart” two-state surface, whose wetting properties and mass throughput (under the application of a pressure gradient) may be tuned by changing the bulk pressure.

The dynamical response of the micro-channel is investigated by applying a constant pressure gradient. In Fig. 5, we show the mass flow rate as a function of the degree of roughness, $a/(L_x - a)$, for a fixed groove depth h and at a given normalized pressure drop, $\Delta P_{lv} h / \sigma_{lv} = 0.75$. The main result here is the presence of a transition at a critical roughness, $a/(L_x - a)$, where the mass flow rate starts to increase with respect to the perfect wetting situations reaching as much as 100% gain. The strong dynamical effect of the gas-layer can be quantified in more detail by inspecting the velocity and momentum profiles along the vertical direction without the vapor layer (fully-wetted configuration) and with a thin vapor layer starting to accumulate close to the bottom of the groove. This is shown in the inset of Fig. 5 where the *local* slip length is also depicted by extrapolation of the bulk profile inside the wall. As soon as a vapor layer is formed, the *local* slip-length ramps-up, reaching values of the order of the channel height $45\Delta x \sim 15nm$. Even larger values can be measured close to the dewetting transition, where a well-developed vapor layer is formed inside the groove (the so-called *super-hydrophobic regime*).

Summarizing, we have shown that an extension of lat-

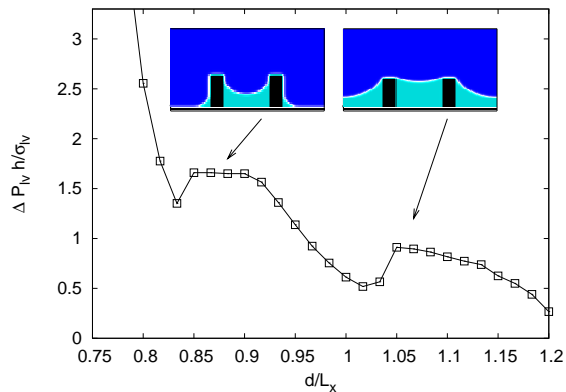


FIG. 4: Pressure variations at changing d , with fixed total mass for the case of heterogeneous roughness (see right panel of Fig. 1). The two plateaux correspond to the case in which the liquid is starting to invade the widest groove (right) and when it is invading also the thinnest (left).

tice Boltzmann equation for non-ideal fluids, can *quantitatively* account for the concerted effects between wetting phenomena and geometrical irregularities. In particular, the presence of nano/micro-irregularities in the flow geometries leads to sizeable effects with respect to the *infinite volume* liquid-gas transitions, as well as to a significant reduction of mechanical drag on the flowing fluid. The consequence of our results is twofold: from a theoretical perspective, it indicates that drag-reduction via geometry-induced wetting transitions is a non-specific phenomenon. On the practical side, the present LBE approach offers the opportunity to perform very efficient numerical simulations of complex micro/nanofluidic phenomena at scales of direct experimental relevance, which are hardly accessible to atomistic simulations. This will open the way to the systematic optimization of microfluidic devices via computer simulation. Useful discussions with J.-L. Barrat, X. Shan and S. Troian are kindly acknowledged.

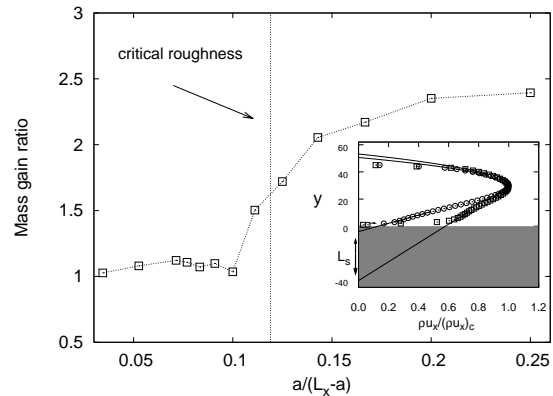


FIG. 5: Mass flow rate normalized to fully wetted case vs the effective roughness $a/(L_x - a)$. The bulk pressure is fixed to be $\Delta P_{lv} = 0.75\sigma_{lv}/h$. A critical roughness (vertical line) is given by the estimate of the capillary pressure, $0.75 \frac{a}{2h \cos(\theta)} = 0.119$ for $a = 10\Delta x$, $h = 33\Delta x$, $\theta = 158^\circ$. Inset: Vertical momentum profile for a wetted (\circ), and almost dewetted configuration (\square). The geometry is fixed to the one of the left panel of Fig. 1 with parameters $h = 14\Delta x$, $a = 14\Delta x$, $L_y = 45\Delta x$, $L_x = 90\Delta x$. Both momentum profiles are shown for $x/L_x = 0.1$ and normalized with their center channel values. The straight lines correspond to extrapolations of the profiles inside the boundaries, i.e. the standard way to define a slip-length.

[1] Cottin-Bizonne, C. Barrat, J.-L. Bocquet, L. & Charlaix, E. *Nature Mater.* **2**, 237 (2003).
[2] E. Lauga, M.P. Brenner & H.A. Stone *Handbook of Experimental Fluid Dynamics*, Springer, New-York (2005).
[3] Y. Zhu & S. Granick *Phys. Rev. Lett.* **88** 106102 (2002); *Phys. Rev. Lett.* **87**, 096105 (2001).
[4] J. Ou & J.P. Rothstein *Phys. Fluids* **17** 103606 (2005).
[5] C. Cottin-Bizonne *et al. Eur. Phys. J. E* **9**, 47-53 (2002).
[6] J.T. Cheng & N. Giordano *Phys. Rev. E* **65**, 031206 (2002).
[7] K. Watanabe & Y.H. Udagawa *J. Fluid Mech* **381**, 225 (1999).
[8] Baudry, J. *et al. Langmuir* **17**, 5232 (2001).
[9] L. Bocquet & J.-L. Barrat *Phys. Rev. Lett.* **70**, 2726

(1993); P. Thompson & S. Troian *Nature* **389**, 360 (1997); N.V. Priezjev *et al. Phys. Rev. E* **71**, 041608 (2005).
[10] E. Lauga & M.P. Brenner *Phys. Rev. E* **70**, 026311 (2004).
[11] D.C. Tretheway & C.D. Meinhart *Phys. Fluids* **16**, L9 (2002).
[12] R. Benzi *et al. Europhys. Lett.* in press, physics/0507026 (2006).
[13] J.W.G. Tyrrell & P. Attard *Phys. Rev. Lett* **87**, 176104 (2001).
[14] S. Granick, Y. Zhu & H. Lee *Nature Materials* **2**, 221 (2003).
[15] S. Chen & G. Doolen *Ann. Rev. Fluid Mech.* **30**, 329 (1998).
[16] R. Benzi, S. Succi & M. Vergassola *Phys. Rep.* **222**, 145 (1992).
[17] C. Cottin-Bizonne *et al. Eur. Phys. J. E* **15**, 427 (2004).
[18] R. Benzi *et al. Jour. Fluid. Mech.* submitted (2006) nlin.CD/0602008.
[19] P.L. Bhatnagar, E. Gross & M. Krook *Phys. Rev.* **94**, 511 (1954).
[20] X. Shan & H. Chen *Phys. Rev E* **47**, 1815 (1993); *Phys. Rev E* **49**, 2941 (1994).
[21] I. Karlin, A. Ferrante & H.C. Oettinger *Europhys. Lett.* **47**, 182, (1999).
[22] B. Li & D. Kwok, *Phys. Rev. Lett.* **90** 124502 (2003).
[23] J. Harting, C. Kunert & H.J. Herrmann, "Lattice Boltzmann Simulations of apparent slip in hydrophobic microchannels" physics/0509035
[24] B.M. Boghosian *et al. Proc. Roy. Soc. Lon.* **A457** 717 (2001).

- [25] S. Ansumali & I.V. Karlin *Phys. Rev. E* **66** 026311 (2002).
- [26] R. Benzi et al. *Jour. Fluid. Mech.* **548**, 257 (2006).